ON ELECTRICAL PROPERTIES OF THERMALLY GROWN Al_2O_3 BASED MIM SANDWICHES

by

RAJESH KUMAR

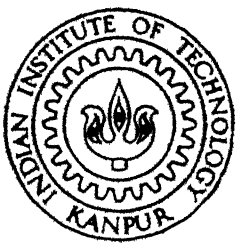

MATERIALS SCIENCE PROGRAMME

INDIAN INSTITUTE OF TECHNOLOGY KANPUR

December, 1996

ON ELECTRICAL PROPERTIES OF THERMALLY GROWN Al_2O_3 BASED MIM SANDWICHES

A thesis submitted

in Partial Fulfilment of the Requirements

for the Degree of

MASTER OF TECHNOLOGY

by

RAJESH KUMAR

to the

MATERIALS SCIENCE PROGRAMME

INDIAN INSTITUTE OF TECHNOLOGY, KANPUR

December, 1996.

CERTIFICATE

It is certified that the work contained in the thesis entitled *"On electrical properties of thermally grown Al_2O_3 based MIM sandwitches"*, Mr. Rajesh Kumar has been carried out under my supervision and that this work has not been submitted elsewhere for a degree.

December, 1996

Jitendra Kumar

(Jitendra Kumar)

Professor

Materials Science Programme

Indian Institute of Technology

Kanpur

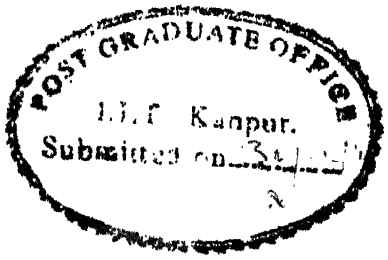

ACKNOWLEDGEMENTS

With profound pleasure, I would like to express my sincere gratitude to Dr. Jitendra Kumar for his invaluable guidance, cooperation and being a constant source of inspiration during the course of this investigation. The completion of this thesis has been possible, only due to his constant intellectual support.

I am deeply indebted to Mr. Subhash Chand for his supportive cooperation, constructive criticism and providing a better technical insight into the functioning of various machines and instruments during thesis work.

Special thanks are due to Anand Madhukar for all the discussions and conversations with him regarding the work have helped a lot.

I would also like to thank Lakhmani, Nayan, Rajneesh, M.K. Singh, Pragya, Prakash, Pankaj, Rajeev and all other friends who, with their good wishes for me, have made my stay here a memorable one.

I thank all the staff members at ACMS and those who have helped me directly or indirectly in the work.

RAJESH KUMAR

Dedicated
to
my parents

CONTENTS

LIST OF FIGURES

Fig. 2.4 Set-up for barrier thickness measurement.

Fig. 3.1 Typical schematic diagram of current density-voltage (J-V) characteristics of Al-Al_2O_3-Al structure showing three distinct regions.

Fig. 3.2 Current density-voltage (J-V) plots for Al-Al_2O_3-Al structures with oxide grown thermally in air at various temperatures.

Fig. 3.3 Current density-voltage (J-V) plots for Al-Al_2O_3-Al with thermally grown oxide at low voltage range to highlight the Ohmic region.

Fig. 3.4 Logarithmic plot of the current density (J) versus square rootof applied voltage ($V^{1/2}$) for Al-Al_2O_3-Alstructures using data of Fig. 3.2.

Fig. 3.5 Plot of ln(J/V) versus $V^{1/2}$ for Al-Al_2O_3-Al structures usingdata of Fig. 3.2.

Fig. 3.6 Plot of $\ln(J/V^2)$ versus V^{-1} for Al-Al_2O_3-Al structures using data of Fig. 3.2.

Fig. 3.7 Plots showing insulator thickness versus oxidation temperature.

LIST OF TABLES

ABSTRACT

An effort has been made to fabricate Al-Al_2O_3-Al sandwiches by growing intermediate oxide layer by thermal oxidation of top portion of aluminium films(thickness ~ 0.25μm) in the temperature range 50-200°C for 24h each and depositing the top aluminium electrodes by thermal evaporation in vaccum and study their electrical characteristics. Their current density-voltage(J-V) data have been analyzed to identify the underlying conduction processes together with respective voltage ranges of operation. Accordingly, Ohmic and Schottky emission are shown to be responsible for current at different voltage regimes depending on the oxide thickness with transition to tunneling occurring at a particular field ~ 10^6 V/cm. The activation energy for Schottky emission and field assisted tunneling processes are demonstrated to increase with the oxide thickness and lie in the range 0.82-0.87eV and 1.73-1.85eV, respectively. The oxide thickness values obtained from J-V data in the Schottky emission and field assisted tunneling regions are found (i) to be quite consistant (ii) lie in the range 20-50 Å, and (iii) increase linearly with the oxidation temperature(50-200°C). The capacitance measurements suggest the presence of the interfacial capacitance ~ 0.74 $\mu F/cm^2$ associated with the oxide and only then lead to thickness values in agreement with those obtained from the J-V characteristics. Further, it is demonstrated that the electrolytic method invariably gives unusually small values of oxide thickness and is perhaps sensitive to a very special region only. Finally, the

electron effective mass is evaluated and shown to decrease with the increase in the oxide thickness.

INTRODUCTION

The studies of metal-insulator-metal (MIM) structures have been stimulated by attractive possibilities of development of a variety of miniaturised solid state devices such as diodes, hot electron triodes, switches, fixed and variable capacitors, piezoelectric transducers, photocells and electroluminiscent devices [1-6]. These active devices are based mainly on the passage of the current through thin layer of poorly conducting materials . As a consequence, interests aroused for identifying conduction mechanisms in thin insulating films [7-13] of SiO, SiO_2, Al_2O_3, BeO, TiO_2, CdS etc., which were previously used as insulators or semi-conductors only. The quest for practical applications has yielded information on their electric behaviour, dielectric breakdown, band structure, potential barriers at the interfaces and current transport at high fields (10^5-10^7 V/cm). The available information is, however, by no means complete or totally consistent. Therefore, it becomes imperative to make a detailed study of the conduction mechanisms [14] in such insulating films. Current voltage-characteristics of thin insulating films (thickness less than 100 Å) have become an important tool for the investigation of electron transport mechanisms. In the past, different workers have shown that currents through thin insulating films and the associated mechanisms oprating depend upon the thickness of the insulator, interface barrier height, temperature and the nature of the

contact between the metal and the insulator [15,16,10].

Simmons [17] has derived current voltage expressions for very thin insulating layer, sandwitched between similar and dissimilar metal electrodes and predicted linear(i.e. Ohmic) and an exponential behaviour at low and high voltages, respectively. He has also studied the MIM structures on the basis of both thermionic emission and tunneling for different values of barrier parameters. Accordingly, below 300 K and for a barrier thickness of less than 40 Å, the conduction is predominantly by tunneling process. However, for thickness greater than 40 Å, current may arise due to thermionic emission and/or tunneling depending upon the barrier height and the applied voltage. Experiments [18] have shown that the current through alumina thin films is mainly due to tunneling but becomes thermionic in nature and obeys $\ln(J)-V^{1/2}$ law beyond a thickness of 50 Å. In relatively thicker films evidence for space-charge limited current has also been found [19]. Hickmott[20] observed a voltage controlled negative registance and switching in such films at high voltages.

1.2 *Nature of MIM interfaces and potential barrier shapes*

When an insulator is sandwiched between two similar metal electrodes the equilibrium condition usually requires that the top of the insulator band gap be positioned between the Fermi level and the vacuum level of the electrodes. Thus, the action of the insulator is to lower the potential barrier (ψ) existing between the two electrodes by an amount $\psi-\phi_o$, where ϕ_o is the distance between the bottom of the insulator conduction band and

the Fermi level of the metal electrodes. Thus, a barrier of height ϕ_o and thickness (s) exists between the two metal electrodes (see, e.g. Fig1.1(a)).

When a potential difference V is applied, the Fermi level of the negatively biased electrode moves vertically upwards by an energy of eV . The barrier height $\phi(x)$ that exists between the electrodes varies continuously within the insulator and the barrier takes a trapezoidal shape if insulator is believed to be homogeneous (see e.g. Fig. 1.2 b). $\phi(x)$ is then given by[21]

$$\phi(x) = \phi_o - \frac{eV}{s}x \qquad \ldots\ldots 1.1$$

This is the case of abrupt potential barrier at the metel-insulator interfaces, which is physically unrealizable and implies infinite forces. Actually an electron between two parallel and closely spaced plates polarizes both of the electrodes and feels the force termed as image force. This, in turn, influences the potential of the electrons in between the electrodes. The image force effect further modifies the barrier (fig. 1.2) with regard to rounding off the edges and decreasing width and height both. The resulting barrier is given by [22]

$$\phi = \phi_o + \phi_i \quad \text{where}$$

$$\phi_i = -\frac{e^2}{8\pi K\varepsilon_o}\{(1/2x)+\sum_{n=1}[ns/((ns)^2-x^2)-(1/ns)]\} \qquad ..1.2$$

and assumes a maximum value at $x = \frac{s}{2}$, such that

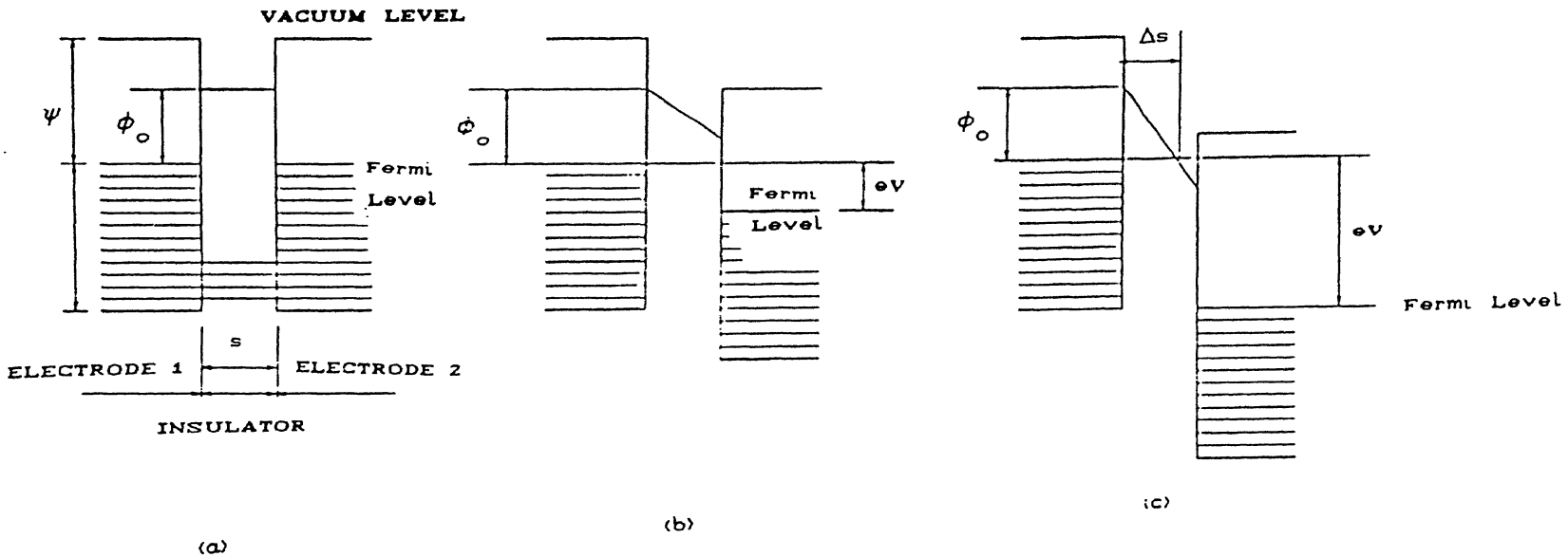

Fig. 1.1 Rectangular potential barrier in insulating fil between metal electrodes for : (a) $V \cong 0$; (b) $V < \phi_o/e$; and (c) $V > \phi_o/e$.

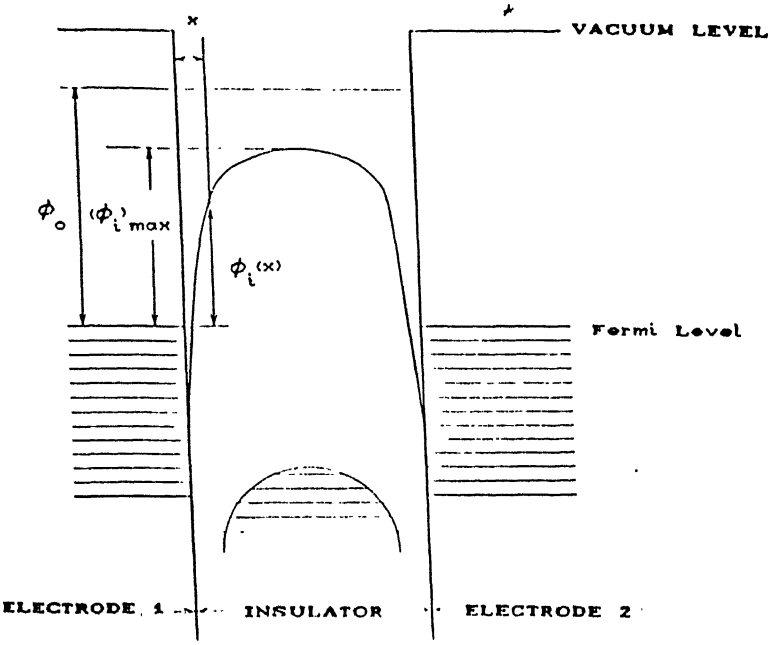

Fig. 1.2 Effect of image force on a rectangular barrier.

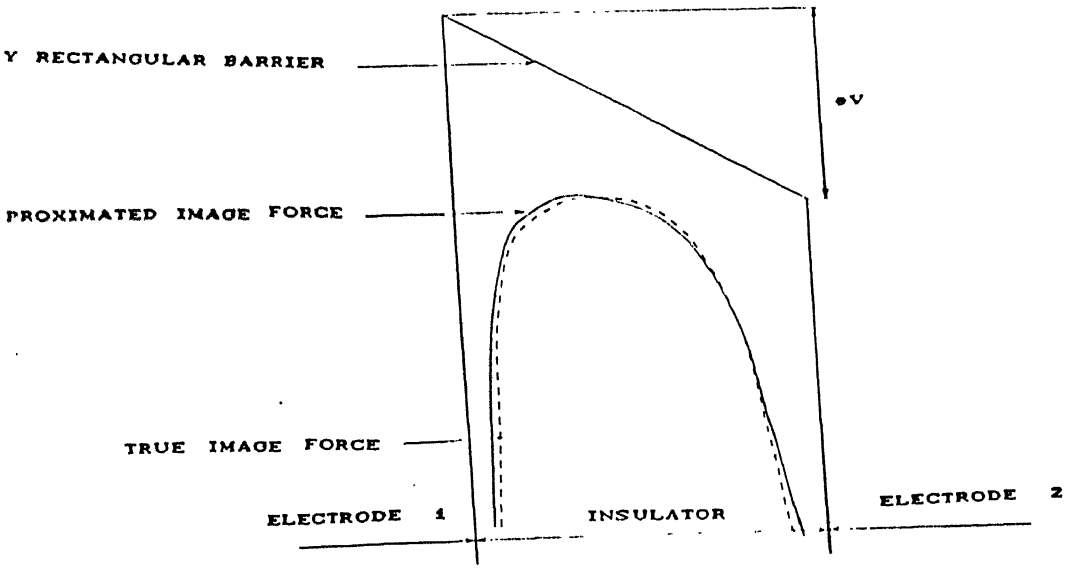

Fig. 1.3 Normalised energy diagram of rectangular barrier with image forces included at some applied voltage V.

$$\phi_{max} = \phi_o - \frac{e^2}{8\pi K\varepsilon_o s} \ln 2 \ . \qquad .....1.3$$

where K is the dielectric constant and ε_o is the permitivity of free space. If ϕ_{max} and ϕ_o are taken in eV and s in angstrom unit, we have

$$\phi_{max} = \phi_o - \frac{10}{Ks} \quad eV \qquad .....1.4$$

At a potential of V volts, the energy band diagram appears as shown in Fig. 1.3. and the resultant potential barrier can be written in the form [17]

$$\phi_I = \phi_o - [2.88s/(Kx(s-x))] - \frac{eVx}{s} \quad eV \qquad .....1.5$$

The image potential on the left and right half of the insulator can be approximated by [17]

$$\phi_{iL} = -[(3.6/Kx)+(7x/s^2K)] \qquad .....1.6$$

and $$\phi_{iR} = -[(3.6/K(s-x)+(7(s-x)/s^2K)] \qquad .....1.7$$

when the electrode 1 is negatively biased, the barrier maximum lies on left half of the insulator. By maximizing ϕ_{iL}, i.e. eqn (1.6), we get

$$x_{oL} = s\,[3.6/(7+eVKs)]^{1/2} \qquad ....1.8(a)$$

$$(\phi_{iL})_{max} = \phi_o - [(14.4(7+eVKs)^{1/2})/Ks] \quad .....1.8(b)$$

If x_o and $(\phi_i)_{max}$ are measured with respect to the positively baised electrode, we have

$$x_{oL} = s - s\,[3.6/(7+eVKs)]^{1/2} \quad .....1.9(a)$$

$$(\phi_{iL})_{max} = \phi_o - [(14.4(7+eVKs)^{1/2})/Ks\ ] \quad .....1.9(b)$$

1.3 *Conduction Mechanisms*

On application of electric field across the MIM structure, the current flows. One now wants to know the contributions to the total current and identify the rate limiting process(es). Electronic conduction through the insulator can be classified into two categories

(a) Barrier limited- thermionic emission, Schottky emission and tunneling.

(b) Bulk limited - space charge limited current, Poole-Frenkel effect, internal field emission and impurity conduction. The important ones of these processes are described below and shown schematically in Fig. 1.4.

It is known that the conductivity in thin insulating films arises due to extrinsically rather than to intrinsically generated carriers. A typical expression for current density through an insulator of band gap E_g and at a temperature T can be written as [22]

$$J = e\mu N_c F \exp[-E_g/kT] \quad ....1.10$$

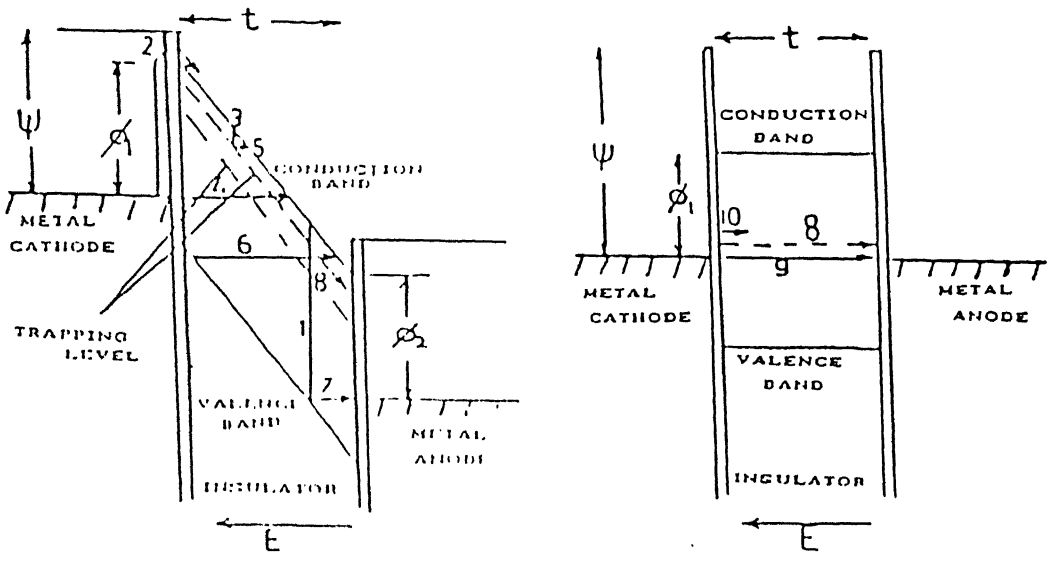

Fig 1.4 Schematic diagram of various conduction processes in MIM structures

1)Electrons raised thermally from valence band if band gap is small and temperature is high;

2)Schottky emission from the metal;

3)Thermal excitation into the conduction band from trap levels in the insulators;

4)Tunneling from metal into the conduction band;

5)Tunneling from trap levels in the insulators;

6)Tunneling directly from valence band to conduction band;

7)Tunneling from valence band of insulator into metal electrode directly;

8)Ionic conduction;

9)Tunneling directly between two metal eletrodes;and

10)Impurity conduction.

where μ is the mobility, F is the field inside the insulator, N_c is the effective density of the states and k is the Boltzmann constant. At room temperature, typical values are $N_c=2.5\times10^{19}cm^{-3}$ E_g = 3 eV, μ = 100 $cm^2V^{-1}s^{-1}$. For F = 10^6 V/cm, current density (J) is about 10^{-18} A/cm^2.

Thus, we find that the electronic current contribution resulting due to the bulk insulator is very small.

1.3.1 *Thermionic emission current*

The thermionic emission current flowing across the MIM junction at a potential V and temperature T is given by the Richardson-Dushman equation [17]

$$J = AT^2 \exp\{-\phi_o/kT\} \exp\left[\frac{[14.4(7+eVKs)]^{1/2}}{KskT}\right] X [1 - \exp(-eV/kT)] \quad ....1.11$$

For large s and eV/kT > 2, eq. (1.11) reduces to

$$J = AT^2 \exp(-\phi_o/kT) \exp[14.4\, eF/K(kT)^2]^{1/2} \quad ..... 1.12$$

where F = V/s is the field in the insulator.

1.3.2 *Schottky emission*

Thermionic emission is a phenomenon in which an electronic current originates from a heated metal. In this case the barrier height is not affected by the applied electric field but gets lowered by the image forces. On the other hand, in Schottky emission process, the applied field itself causes lowering of the

barrier height [22] (Fig. 1.5). The effective work function becomes

$$\phi_E = \phi - \frac{E^{1/2}\, e^{3/2}}{2K^{1/2}} \qquad .....1.13$$

where ϕ is the original work function of the metal electrode. The current density in this case is given by

$$J = AT^2 \exp(-\phi/kT) \exp\left[-\frac{e^{3/2}E^{1/2}}{2(4\pi\varepsilon_o K)^{1/2}\, kT}\right] \qquad .....1.14$$

where $A = \frac{4\pi mek^2}{h^3} = 120\ A/cm^2K$

For numerical evaluations, eq. (1.14)is reduced by substituting the values of constants. Thus,

$$J = 120\, T^2 \exp\left[\left(\frac{3.89\, V^{1/2}}{K^{1/2}\, S^{1/2}} - 1.159\phi\right)\frac{10^4}{T}\right] \qquad .....1.15$$

1.3.3 *Poole-Frenkel effect*

This effect involves a mechanism which is very similar to the Schottky emission, except that it relates to the thermal excitation of electrons from traps into the conduction band of the insulator [22]. The energy diagram for such a trap has been shown in Fig.1.6. In this case the effective barrier height and current density are given by

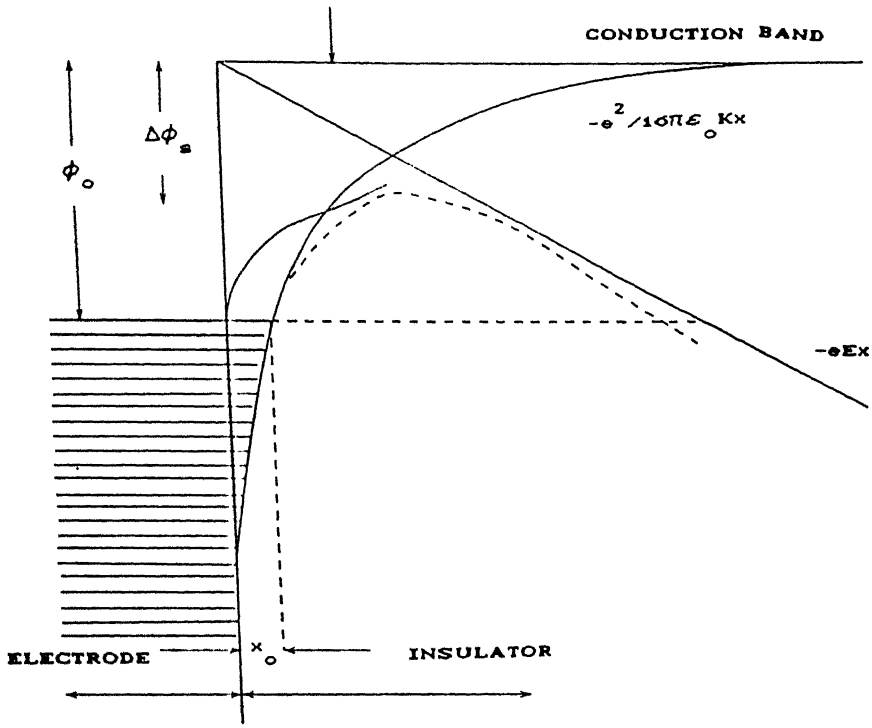

Fig. 1.5 Energy diagram of Schottky effect at neutral contact under applied electric field.

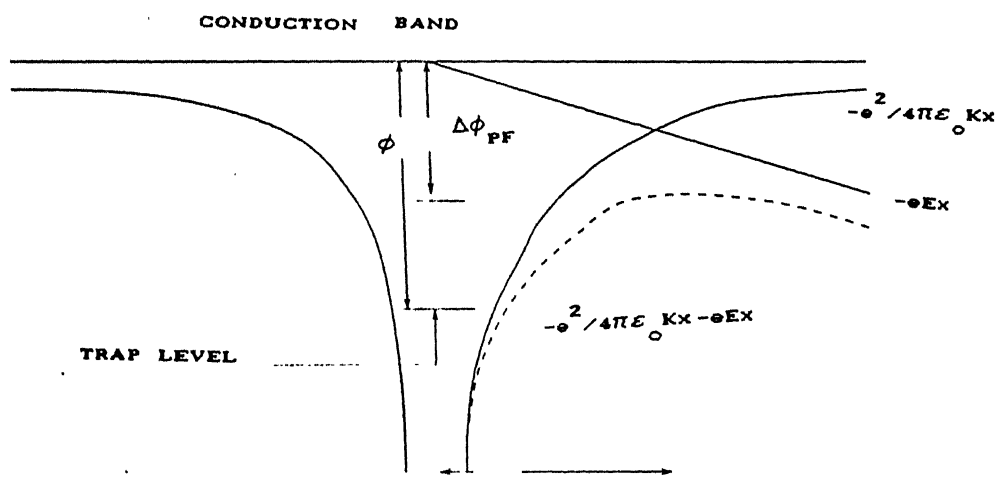

Fig. 1.6 The lowering of the potential barrier for thermal excitation of trap electrons into the conduction band of the insulator by an external electric field.

$$\phi_e = \phi_o - 2\,(e^3E/K)^{1/2}.$$

ıd the current density is given by

$$J = AT^2 \exp(-\phi_o/kT) \exp\left[-\frac{e^{3/2}E^{1/2}}{K^{1/2}\,kT}\right] \qquad .....1.16$$

here $A=\frac{4\pi mek^2}{h^3} = 120$ A/cm^{2}K. For numerical evaluations, eq. (1.16)

jets reduced to

$$J = 120\,T^2 \exp\left[\left(\frac{7.78\,V^{1/2}}{K^{1/2}\,\bar{s}^{1/2}} - 1.159\phi\right)\frac{10^4}{T}\right] \qquad .....1.17$$

1.3.4 *Tunneling*

Electronic current can flow through the insulating film if (a) the electrons in the metal electrode have enough thermal energy to surmount the potential barrier and go into the conduction band of the insulator and/or (b) the barrier is thin enough to permit the penetration of electrons by the so called tunnel effect (Fig. 1.7).

For rectangular barrier, the general expression for the tunnel current is [21]

$$J = J_o\{\bar{\phi}\exp(-A\bar{\phi}^{1/2}) - (\bar{\phi}+eV)\exp[-A(\bar{\phi}+eV)^{1/2}]\} \qquad .....1.18$$

$$\text{where } J_o = \frac{e}{2\pi h\,(\beta\Delta s)^2} \qquad ...1.19$$

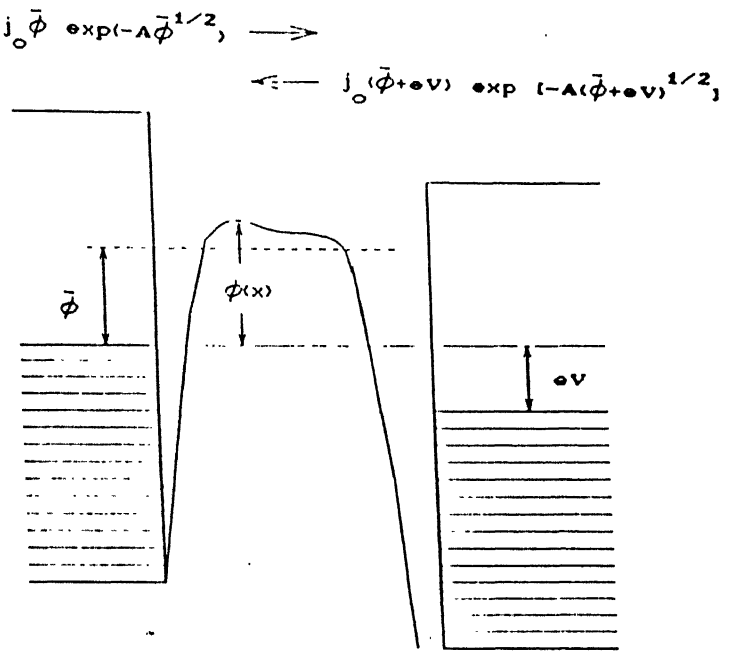

1.7 Pictorial illustration of eqn(1.18), showing current flow between electrodes.

and $\bar{\phi} = \frac{1}{\Delta s} \int \phi(x)\, dx$, with the correction factor (β)

$$\beta = 1 - \frac{1}{8[\eta+\bar{\phi} - E_x]\Delta s} \int [\phi(x)-\bar{\phi}]^2\, dx,$$

$$A = \frac{4\pi\beta\Delta s(2m)^{1/2}}{h} \quad \text{and} \quad \Delta s = s_2 - s_1$$

Three convenient forms of eq. (1.18) can be deduced for low, intermediate and high voltages ranges (Fig. 1.1) as follows :

(a) Low voltage range :

In this case $V \sim 0$, $\beta \sim 1$, $\bar{\phi} = \phi_o > eV$, $\Delta s = s$ and the expression for the current density takes the form

$$J = \frac{(2m)^{1/2}}{s} \left[\frac{e}{h}\right]^2 \phi_o^{1/2} V \exp\left[-\frac{4\pi s(2m)^{1/2}\phi_o^{1/2}}{h}\right]$$

$$= 3.16 \times 10^{10} \frac{\phi_o^{1/2} V}{s} [\exp - 1.025\, s\phi_o^{1/2}] \qquad \ldots.1.20$$

where s, ϕ_o and V are in Angstroms, eV and volts, respectively.

(b) Intermediate voltage range :

Here $V \leq \phi_o/e$, $\Delta s = s$, $\beta = 1$ and $\bar{\phi} = \phi_o - \frac{eV}{2}$. The current density is given by

$$J = \frac{e}{2\pi h s^2} \left\{\left[\phi_o - \frac{eV}{2}\right] \exp\left[-\frac{4\pi s}{h}(2m)^{1/2}\left[\phi_o - \frac{eV}{2}\right]^{1/2}\right\}\right.$$

$$\left. -\left\{\left[\phi_o + \frac{eV}{2}\right] \exp\left[-\frac{4\pi s}{h}(2m)^{1/2}\left[\phi_o + \frac{eV}{2}\right]^{1/2}\right]\right\}\right\}$$

$\ldots.1.21$

$$J = 6.2 \times 10^{10} \times \frac{1}{s^2} \left(\left[\phi_o - \frac{eV}{2} \right] \exp \left[-1.025\, s \left[\phi_o - \frac{eV}{2} \right]^{1/2} \right] \right.$$

$$\left. \left[\phi_o + \frac{eV}{2} \right] \exp \left[-1.025\, s \left[\phi_o + \frac{eV}{2} \right]^{1/2} \right] \right)$$

.....1.22

(c) High Voltage Range :

In this case, $V \geq \phi_o/e$, $\bar{\phi} = \frac{\phi_o}{2}$, $\Delta s = s \frac{\phi_o}{eV}$ and $\beta = 23/24$. The current density becomes

$$J = \frac{2.2\, e^3 V^2}{8\pi h \phi_o s^2} \left\{ \exp \left[- \frac{8\pi s}{2.96\, heV} (2m)^{1/2} \phi_o^{3/2} \right] + \left[1 + \frac{eV}{\phi_o} \right] \right.$$

$$\left. \exp \left[- \frac{8\pi s}{2.96\, heV} (2m)^{1/2} \phi_o^{3/2} \left[1 + \frac{2eV}{\phi_o} \right] \right] \right\}$$

.....1.23

$$J = 3.98 \times 10^{10} \frac{V^2}{\phi_o s^2} \left\{ \exp \left[- \frac{0.689}{V} \phi_o^{3/2} \right] + \left[1 + \frac{eV}{\phi_o} \right] \right.$$

$$\left. \exp \left[- \frac{0.689\, s}{V} \phi_o^{3/2} \left[1 + \frac{2eV}{\phi_o} \right]^{1/2} \right] \right\}$$

.....1.24

(d) Very high voltages :

Here $V >> \phi_o/e$, and second term in eqn. 1.22 is negligible. Thus,

$$J = J_o' \left[\frac{2.2\, (eV)^2}{4\phi_o} \right] \exp \left[- \frac{-2A\, \phi_o^{3/2}}{2.96\, eV} \right] \quad \ldots 1.25$$

This is Fowler-Nordheim equation. The situation is analogous to that of field emission from a metal electrode.

1.6 *Objective of the Present Work*

In the present work, an attempt has been made to fabricate Al-Al_2O_3-Al structures by growing the intermediate oxide layer by thermal oxidation in air at 50, 75, 100, 150, 200°C, and study their electrical properties to understand the conduction process(es) involved, and determine various parameters like barrier height, oxide thickness, etc.

CHAPTER 2

EXPERIMENTAL DETAILS AND PROCEDURES

2.1 *Substrate Cleaning*

Glass slides of the size 75mm x 25mm x 1mm have been used as substrates. These slides normally contain contaminants like grease, finger prints, airborne particulate matter, residues from manufacturing and packaging, etc., and so were cleaned with a soap detergent, dipped in chromic acid for some time and throughly rinsed in distilled water. They were then put in trichloro-ethylene, acetone, methanol and distilled water in succession and stirred in an ultrasonic cleaner. Lastly, the slides were dried inside a clean bench, wiped with lint free tissue paper and put in a vacuum desiccator for storage.

2.2 *Sample Preparation*

Fig. 2.1 shows the schematic diagram of various steps involved in the preparation of the Al-Al_2O_3-Al structures.

(a) *Bottom Electrode Preparation* –

Firstly, the masks containing openings of length 75mm and breadths of 0.8, 1.0, 1.25, and 1.5mm were made. Aluminium of 99.99% purity was subsequently deposited(thickness ~ 0.25μm) onto the glass substrate covered by masks by thermal evaporation under vacuum ~ 10^{-6} torr in a work chamber using a tungsten spiral and

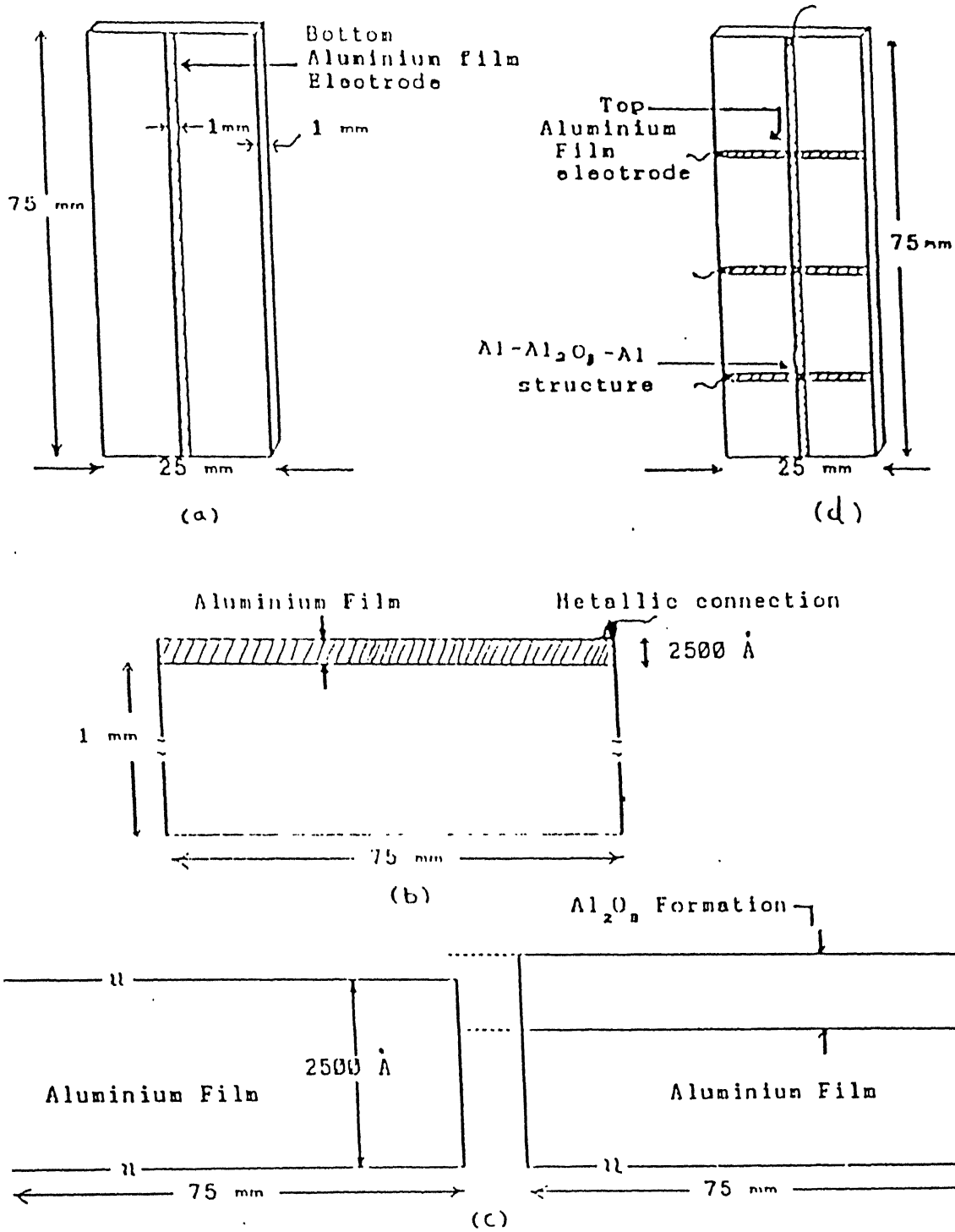

ig. 2.1 Different stages of preparation of Al-Al_2O_3-Al structures.

passing a low voltage-high amperage current for about 10 seconds. The silver paste was applied then at one end of each aluminium strips to protect the so called bottom electrode from thermal oxidation and to make contacts later. (Fig.2.1 a,b)

(b) *Oxide formation* -

An electric furnace equipped with a temperature controller was used for oxidizing the top surface region of aluminium strips. The temperatures selected were 50, 75, 100, 150 and 200°C and oxidation performed for 24h each in air. The process allowed oxidation to occur upto a certain depth depending upon the temperature and yielded oxides of various thicknesses.

(c) Top electrode deposition -

Cross strips of aluminium of thickness about 2500 Å were then deposited in the same manner as described in Section 2.2(a) using another set of masks. Electrical connections were made thereafter using copper wires and silver paste as adhesive.

2.3 *Junction area, capacitance and current-voltage measurements*

Junction area was determined using an image analyser Leitz ASM 68K equipped with a varioscan V16 video camera. The total capacitance of each Al-Al_2O_3-Al structure was measured with a LCR meter HP 4276 at a frequency of 100 Hz and a test voltage of 0.5 volt. Fig 2.2 shows schematically the experimental set-up used for recording current-voltage characteristics. It comprised of a PC-Zenith PC XT 286, a programmable voltage source (Kiethley

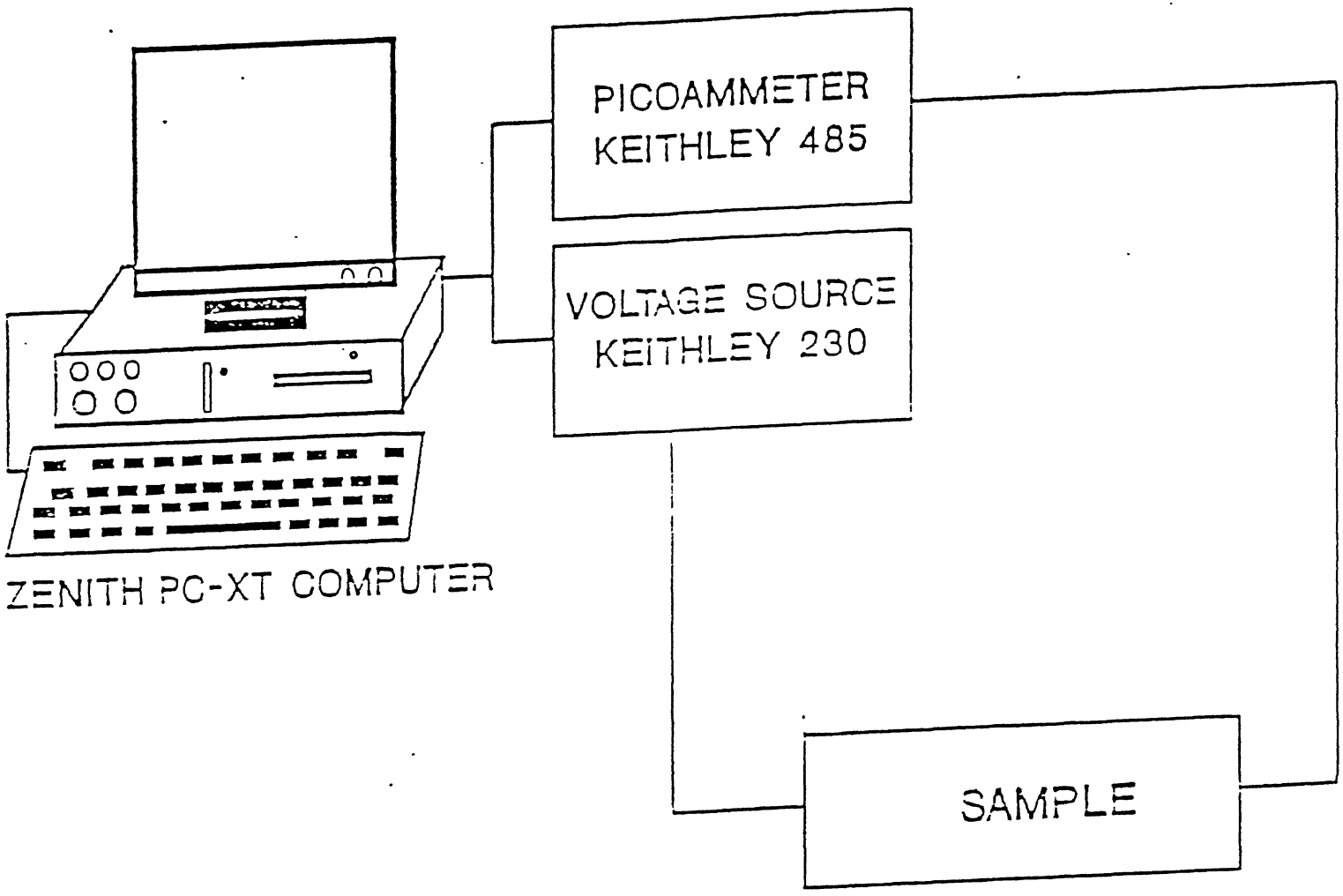

Fig.2.2 Schematic diagram of the automated experimental set-up used for current density-voltage (J-V) measurements.

model 230) and an autoranging picoammeter (Keithley model 485). For measurements, voltage was raised in steps of 0.05V and the current recorded automatically. The circuit diagram of the current-voltage measurements is given in Fig. 2.3.

2.4 *Electrolytic method for measuring the insulator thickness*

An electrolytic method was employed to measure the oxide thickness. In this, the specimen was made the anode and placed in a 3 wt% tartaric acid solution of pH ~ 5.5 (adjusted with NH_4OH). Cathode is just a stainless steel plate. Fig 2.4 shows the electrolytic cell together with the circuit used. The potential applied is increased gradually till a stage reached when the current no longer increases and takes a constant value termed as normal leakage current. The corresponding voltage when multiplied by a factor 14 gives thickness in Angstrom units [23,24].

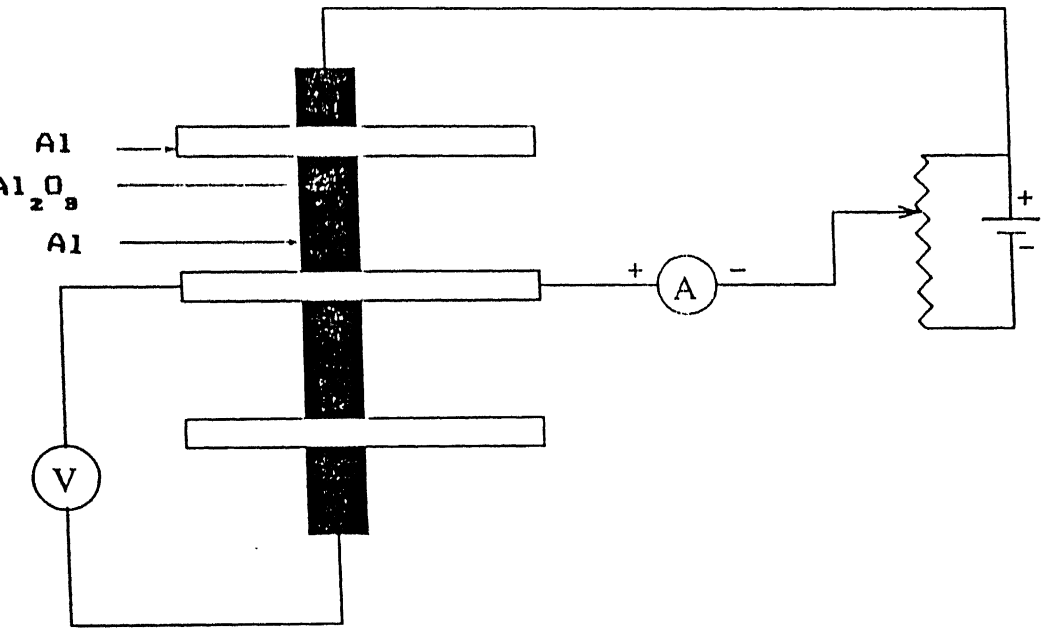

. 2.3 Experimental set-up for current-voltage measurement.

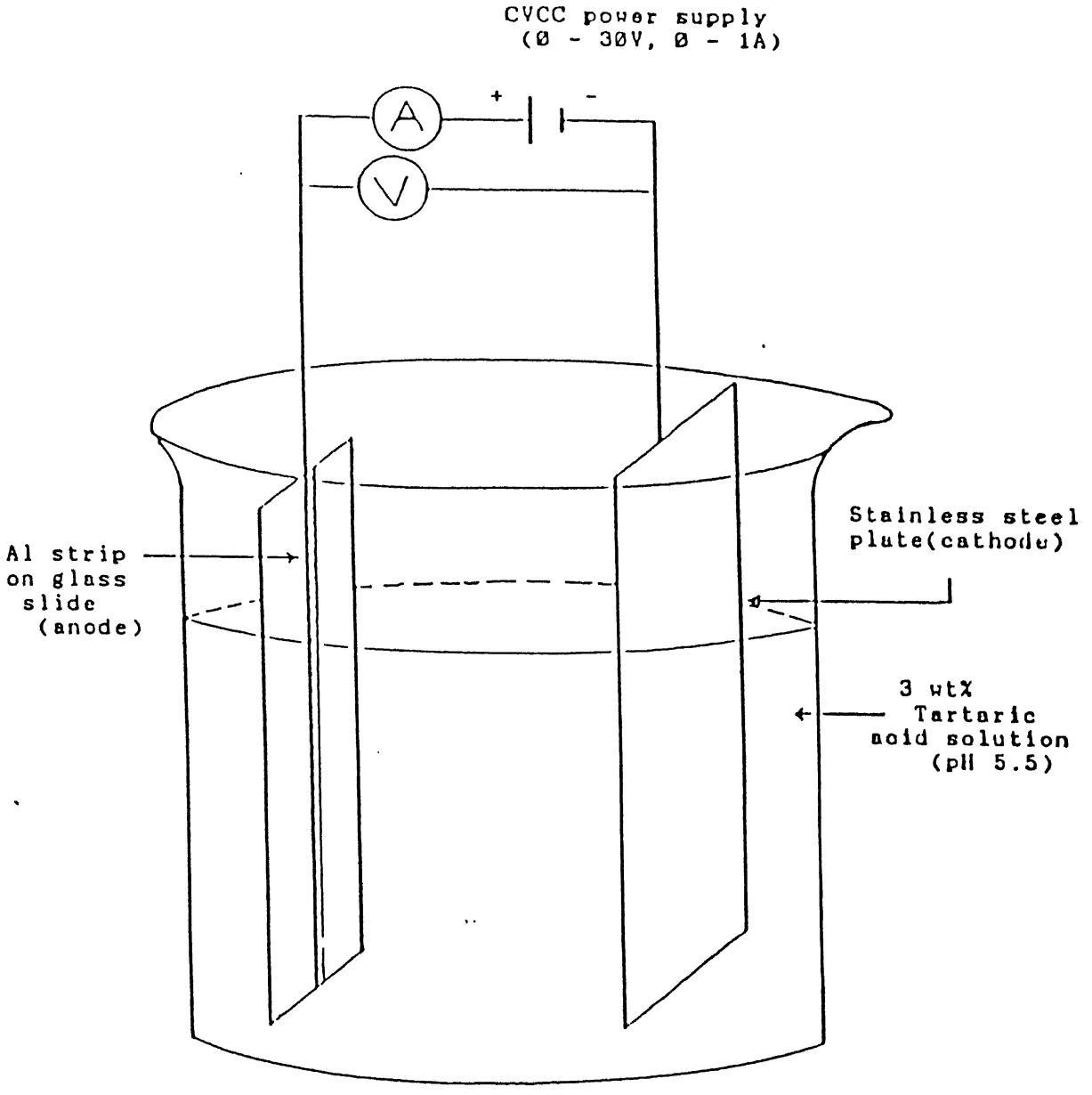

Fig. 2.4 Set-up for barrier thickness measurement.

CHAPTER 3

RESULTS AND DISCUSSION

3.1 *Oxide formation*

The process of initial oxide formation is very complex and involves various physical and chemical processes, e.g., physiosorption, chemisorption, etc. [25]. However, once initial oxidation occures, further growth is sustained by movement of atoms (oxygen and/or aluminium) through the oxide for reaction at the oxide-aluminium and oxide-oxygen interface, respectively. Thus, the rate of further oxidation is governed by the kinetics of the reaction itself. Aluminium oxide is reasonably stoichiometric having a chemical composition Al_2O_3 with low defect concentration. Its specific volume is different from that of the metal consumed and the difference is best represented by Pilling-Bedworth ratio (Φ) defined as

$$\Phi = \frac{\text{Molecular volume of oxide}}{\text{Atomic volume of metal}} = \frac{M_o d_m}{\eta^* M_m d_o}$$

where M_m is the atomic weight of the metal, M_o is the molecular weight of the oxide, η^* is the number of the metal atoms per molecule of the oxide and d_m and d_o are the densities of the metal and the oxide, respectively. The physical significance of Φ lies in quantifying the protective ability of the oxide. If Φ is

less than unity, the oxide fails to cover the entire metal surface and gives rise to a discontinuous layer permitting easy passage to the species. Thus, the amount of the oxide formed depends only on the elapsed time at any given temperature. When Φ is greater than unity, the oxide occupies larger volume than the metal consumed and, therefore, protects the underlying metal. The growth is than controlled by diffusion of oxygen and metal atoms via the oxide layer. The aluminium oxide is always protective in nature. For oxidation temperatures below 450°C aluminium oxide formed is amorphous and quite stable. Its work function is 5.4 eV. Further, Al_2O_3 exhibits ionic bonding and large band gap (7eV).

3.2 Current voltage characteristics

The current density-voltage (J-V) characteristics of Al-Al_2O_3-Al trilayer structures are complex in nature and correspond to a typical trend shown in Fig. 3.1. They depict linearity at low but exponential behaviour at high voltages. In fact, the plot can be divided into three distinct regions : (i) a linear region involving marginal increase in current with voltage and termed as Ohmic, (ii) a non-linear region with moderate and steep rise (by a few orders in magnitude) in current beyond a threshold voltage leading eventually to dielectric breakdown, and (iii) anomalous region at high voltages of very high current followed by negative resistance and fluctuations (or noise) in current. The presence and extent of various regions, however, varies with the oxide thickness.

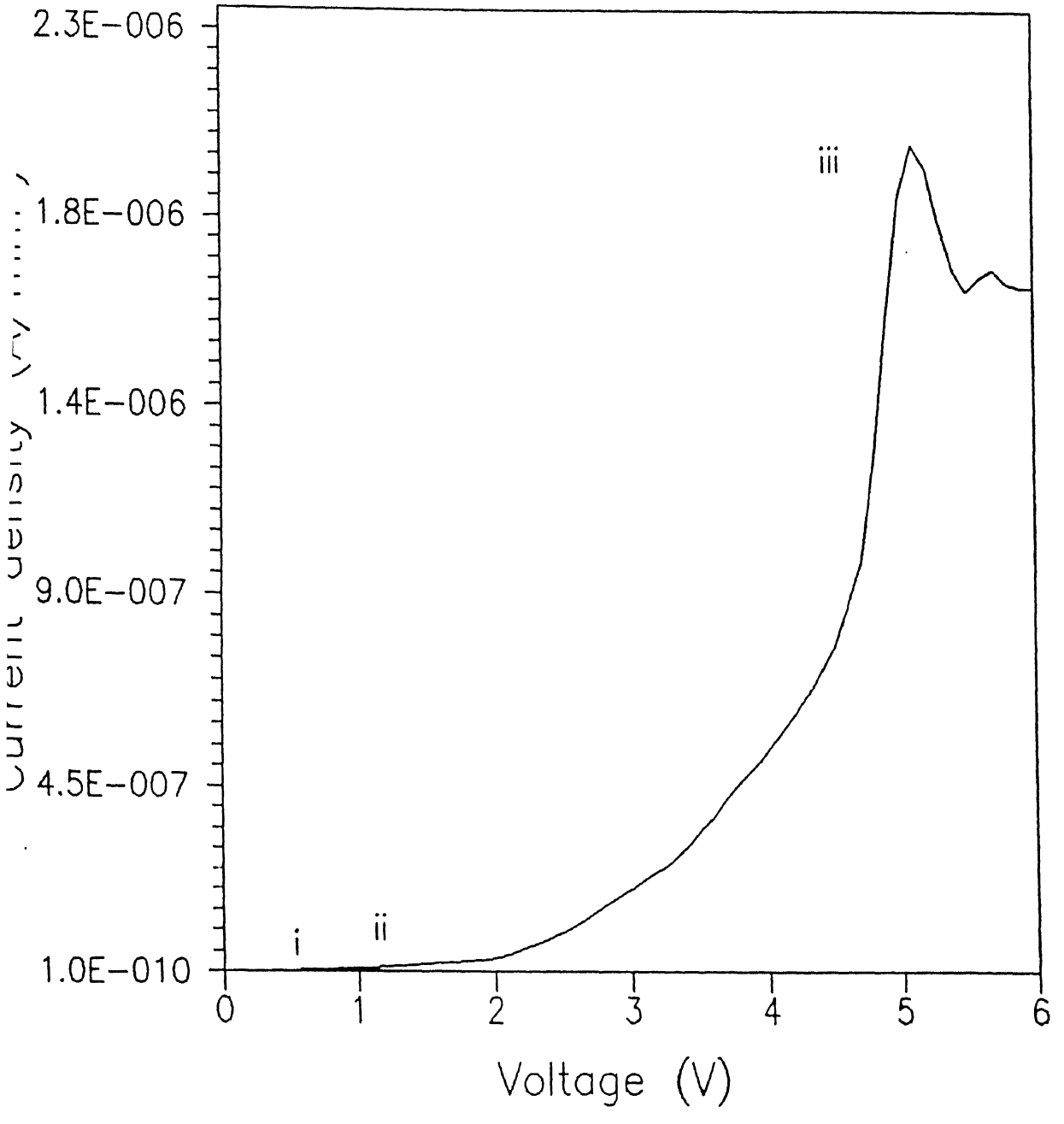

Fig. 3.1 Typical schematic diagram of current density-voltage (J-V) characteristics of Al-Al_2O_3-Al structure showing three distinct regions (i), (ii) and (iii).

3.3 *Analysis of measured data and interpretation*

When the oxide film thickness in a MIM structure is only a few tens of Angstrom, the applied bias as low as 0.1V induces a high electric field ~10^5 V/cm. Associated with such a high electric field is the conduction by one or more of the five principal modes, viz., Ohmic, space-charge limited, tunneling, Schottky emission and Poole-Frenkel effect[14]. These conduction mechanisms may operate simultaneously, but their relative dominance in a particular voltage range depends on the thickness and properties of the insulator. We have plotted the J-V data in various ways to identify the conduction mechanism(s) operating in Al-Al_2O_3-Al structures. Table 3.1 [26] summarises the characteristic features of various conduction mechanisms along with the types of the plots found useful for their identification.

Fig 3.2 shows current density-voltage characteristics of Al-Al_2O_3-Al structures obtained with top electrode as negatively biased. The oxide has been grown in air at temperatures varying from 50 to 200 °C for 24h each. In these plots strong dependence of current density on oxidation temperature is evident. The initial linear regions of these curves have been replotted and shown in Fig.3.3. It is clear that linearity is observed upto a certain voltage, which increases with the increase of the oxidation temperature. However, the transition from the linearity becomes more abrupt. The voltages at which the transition occurs (i.e., threshold voltage) are listed in Table 3.2.

To identify the range in which Schottky emission is

Table 3.1 Characteristics of various conduction processes operating in thin insulating films [26]

Conduction type	Plot(s)	Nature	Remark(s)
Ohmic	J vs V	Linear	Ohm's law $J \propto V$
Space-charge limited	J vs V ln(J) vs ln(V)	Non-linear Linear with slope=2 slope=3	Child's law $J \propto V^2$ Cube law $J \propto V^3$
Tunneling	$\ln(J/V^2)$ vs 1/V	Straight line with negative slope	Fowler-Nordhiem equation, $J=J_o\{2.2(eV)^2/(4\phi_o)\}$ $\exp[-2A'\phi^{3/2}/(2.96eV)]$
Schottky emission	ln(J) vs $\sqrt{V}$	Straight line with positive slope	Richardson-Schottky equation, $J=A^* T^2 \exp(-\phi_o/kT)\exp(e\beta_s V^{1/2}/kT)$ slope gives field lowering coefficient β_s
	$\ln(J/V^2)$ vs 1/V	Curve with a definite minimum	Modified Schottky equation $\ln(J/V^2) = B + B'\sqrt{V} + 2\ln(1/V)$ B and B' are constants
Pool-Frankel effect	ln(J) vs $\sqrt{V}$	Straight line	slope gives field lowering coefficient β_{PF}
	ln(J/V) vs $\sqrt{V}$	Straight line	Pool-Frankel current equation $J = A_{PF}(V/t)\exp(-\phi_o/kT)$ $\exp(e\beta_{PF}V^{1/2}/kT)$ slope gives field lowering coefficient β_{PF}

dominating we make $\ln(J)$ vs $V^{1/2}$ and $\ln(J/V)$ vs $V^{1/2}$ plots (Figs. 3.4 and 3.5). These exhibit linear dependence in certain voltage range in Fig. 3.4 only and therefore suggests the possibility of occurrence of Schottky emission. Fig. 3.6 shows $\ln(J/V^2)$ vs V^{-1} plots. The appearance of a definite minimum in these plots confirms the existence of Schottky emission. The voltage ranges of Schottky emission are listed in Table 3.2. Considering the linearity span of $\ln(J)$ vs $V^{1/2}$ plots and using eq. (1.14) the barrier height and the field lowering coefficient(β_s) have been determined from the intercept and slope, respectively. Since $\beta_s = [e/(4\pi\varepsilon_o Ks)]^{1/2}$, the oxide thickness can be easily found out by taking the value of the dielectric constant for Al_2O_3 as 8.8 [27-29]. The values so obtained are given in Table 3.3. These clearly show a gradual increase in the barrier heights with the insulator thickness, consistent with other observations [27,29].

The $\ln(J/V^2)$ versus V^{-1} plots show straight lines with negative slope at voltages beyond the definite minimum. This region corresponds to field assisted tunneling. From the slopes and intercepts we can estimate the barrier height and oxide thickness again using eq. (1.25). These values have been listed in Table 3.4. Notice excellent agreement in the thickness values obtained from Schottky emission and tunneling data. The activation energy for field assisted tunneling is invariably higher. Interestingly, barrier height (ϕ) also increases with the oxide thickness. Further, the transition to tunneling is occurring at a field of $\sim 3.3\times10^6$ V/cm, irrespective of the oxide

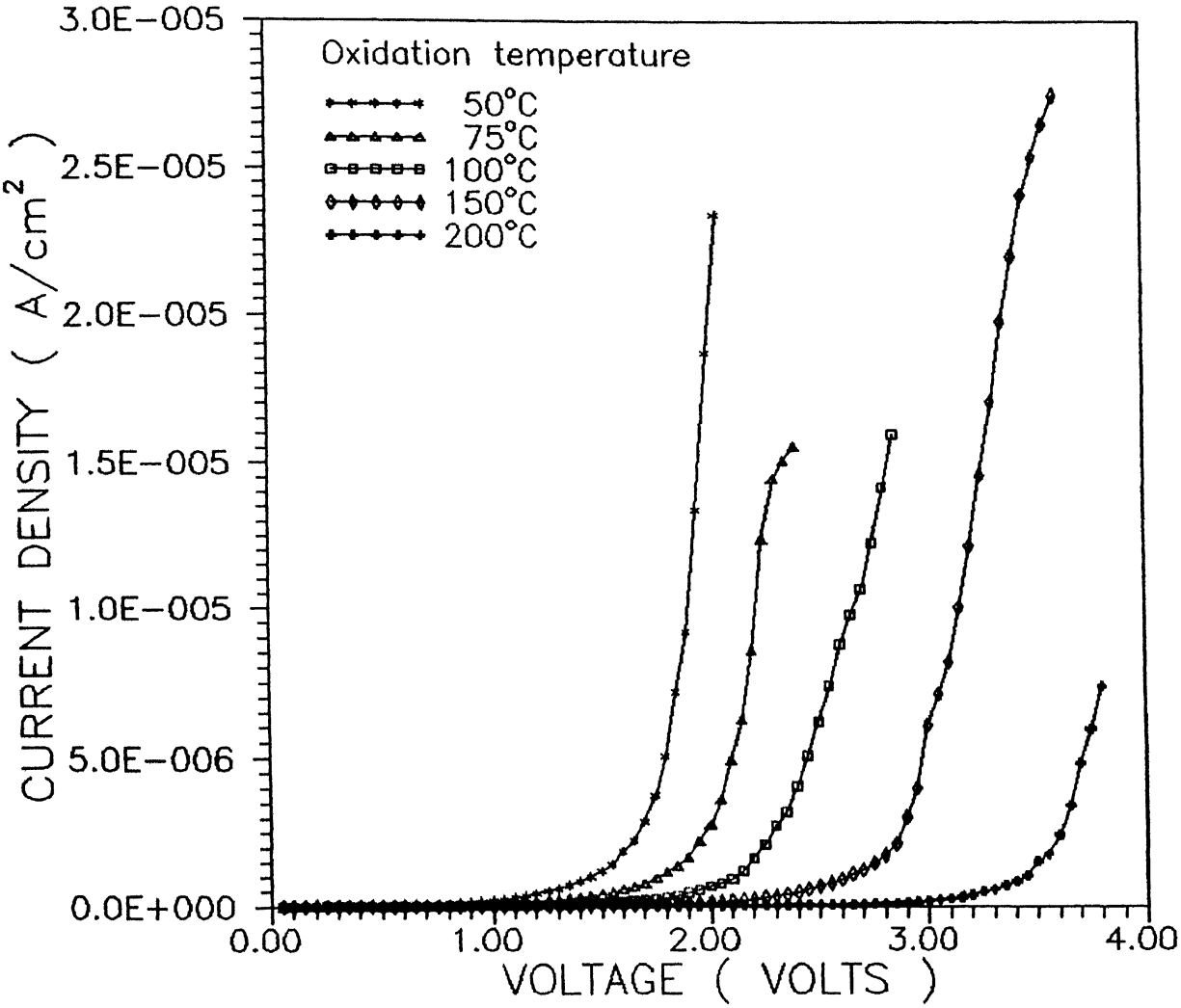

Fig. 3.2 Current density-voltage (J-V) plots for Al-Al_2O_3-Al structures with oxide grown thermally in air at various temperatures.

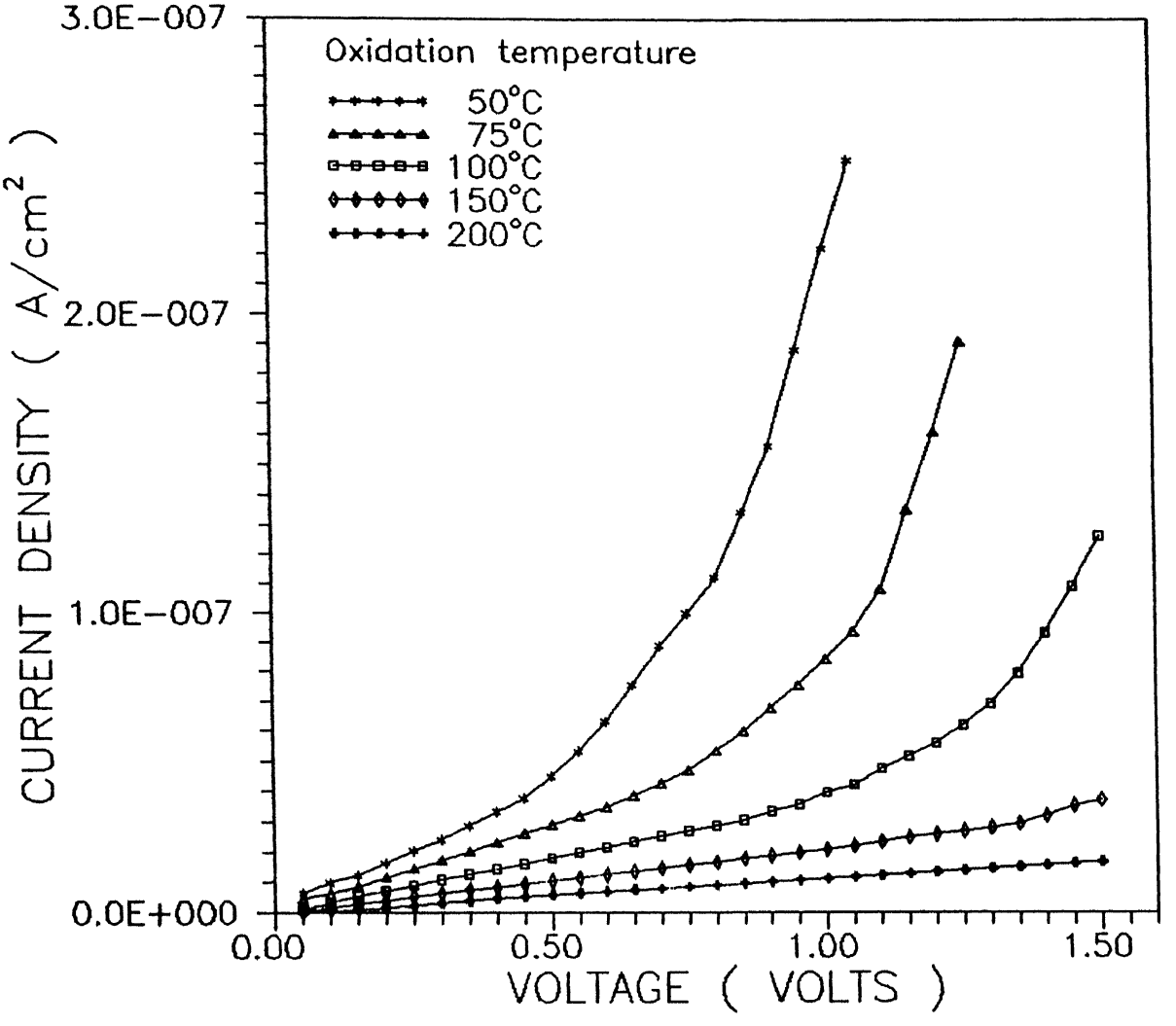

Fig. 3.3 Current density-voltage (J-V) plots for Al-Al_2O_3-Al with thermally grown oxide at low voltage range to highlight the Ohmic region.

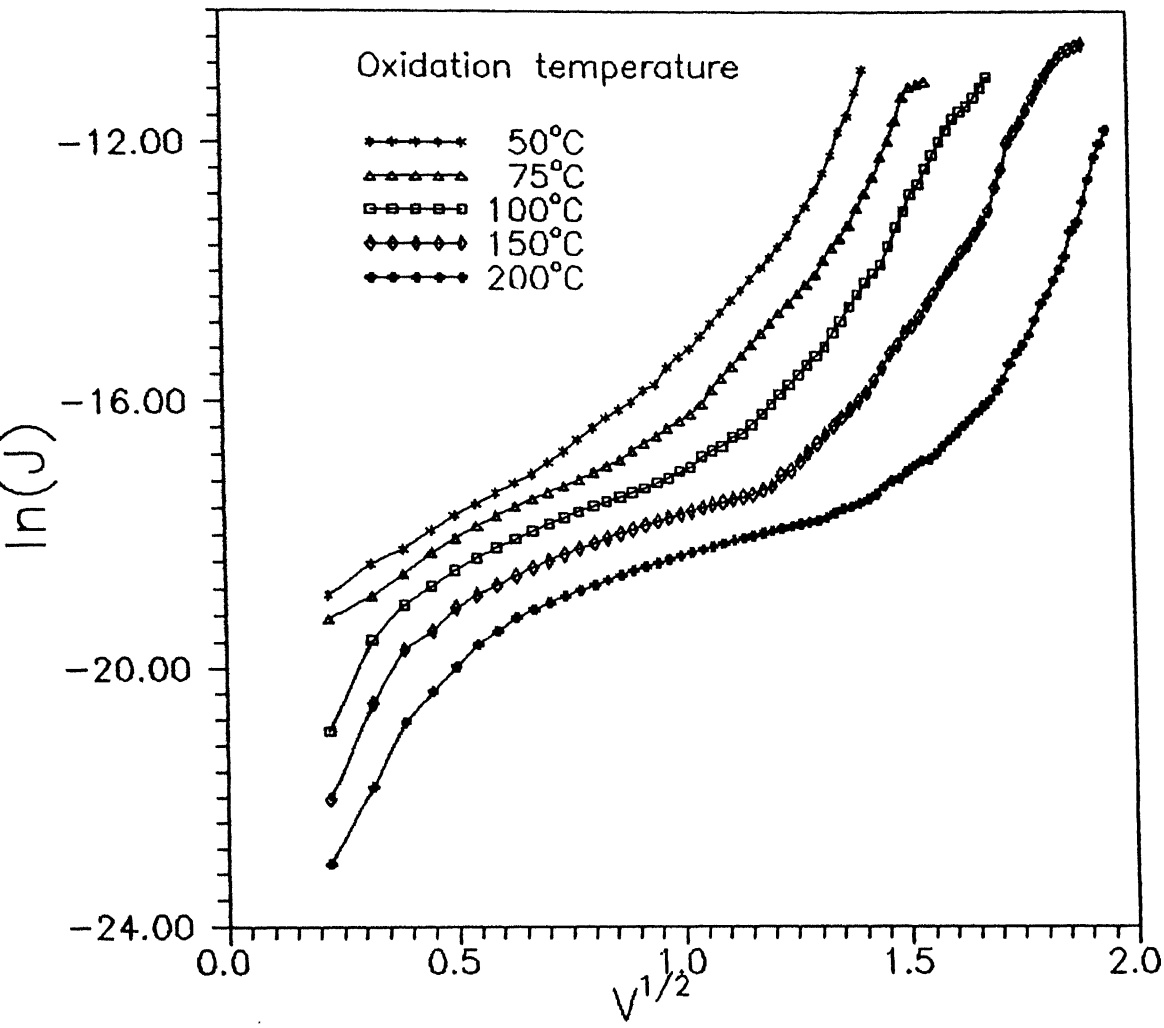

Fig. 3.4 Logarithmic plot of the current density (J) versus square root of applied voltage ($V^{1/2}$) for Al-Al_2O_3-Al structures using data of Fig. 3.2.

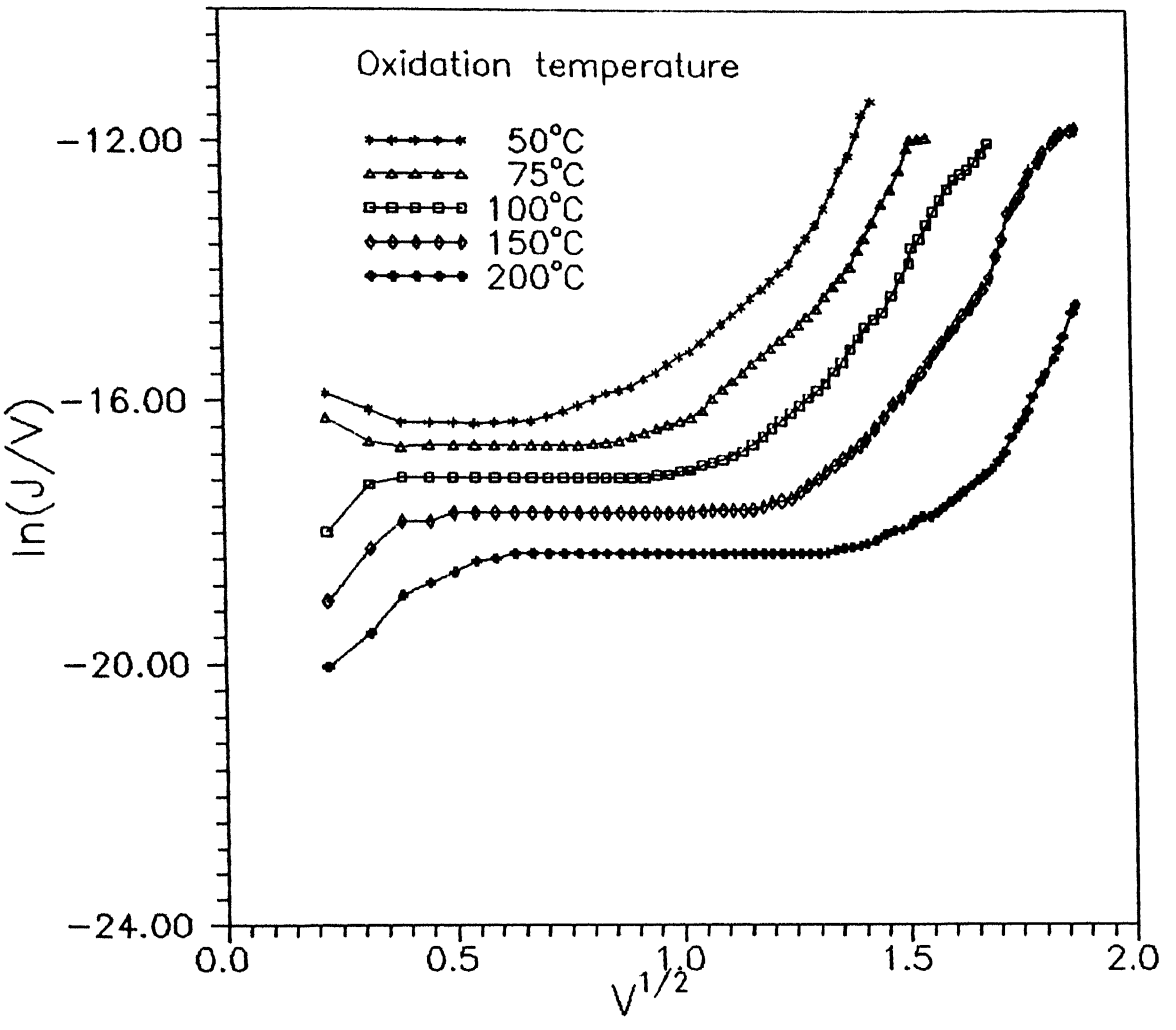

Fig. 3.5 Plot of ln(J/V) versus $V^{1/2}$ for Al-Al_2O_3-Al structures using data of Fig. 3.2.

Table 3.2 Voltage ranges for different conduction processes

Oxidation Temperature (°C)	Ohmic (V)	Schottky Emission (V)	Field assisted Tunnling (V)
50	<0.40	0.40 - 1.30	>1.30
75	<0.60	0.60 - 1.70	>1.70
100	<0.80	0.80 - 1.95	>1.95
150	<1.35	1.35 - 2.20	>2.20
200	<1.65	1.65 - 2.75	>2.75

Table 3.3 Values of insulator thickness(s_s) and barrier he
energy(ϕ) in the Schottky emission range for var
Al-Al_2O_3-Al structures

Oxidation Temperature (°C)	$\beta_s(V^{1/2})$	s_s(Å)	ϕ(eV)
50	0.23	23	0.82
75	0.22	27	0.82
100	0.21	33	0.84
150	0.19	45	0.84
200	0.18	49	0.87

Table 3.4 Estimated values of s_T and ϕ in the tunneling regio

Oxidation Temperature ($^{\circ}$C)	s_T(Å)	ϕ(eV)
50	24	1.73
75	29	1.75
100	35	1.81
150	46	1.83
200	50	1.85

Table 3.5 The values of oxide thickness(in Å) as determined by capacitance measurements and electrolytic method.

Annealing Temperature ($^{\circ}$C)	Oxide thickness obtained (in Å)		
	Using capacitance data with K = 8.8		by Electrolytic Method
	C_i/A = 1.37 $\mu F/cm^2$	$C_i/A = \infty$	
50	48	96	7
75	56	104	9
100	65	113	12
150	76	124	18
200	86	134	25

thickness.

3.4 *Estimation of oxide thickness*

The estimation of the dielectric thickness has been done
adopting three different methods i.e. electrolytic method,
Schottky range and using capacitance data. Obtained values ha
been plotted in Fig. 3.7. Dielectric thickness has be
determined by assuming the total measured capacitance C_m to ha
contribution of bulk of thickness s (i.e. geometric capacitan
say, C_b) and an interfa-cial capacitance C_i lying in seri
[20,30]. The capacitance associated with the bulk dielectric c
be wrtten in the form

$$C_b = \frac{K\varepsilon_o A}{s} \qquad \text{.....3}$$

where K is the dielectric constant and A is the area of t
dielectric. Thus, the reciprocal areal capacitance should have
linear dependance on s with a nonzero intercept at s=0, i.e.,

$$\frac{A}{C_m} = \frac{A}{C_i} + \frac{s}{\varepsilon_o K} \qquad \text{.....3}$$

On this basis, the dielectric thickness has been found for
sets of the samples with oxide layers grown at temperatu
50,75,100,150 and 200 °C using C_i/A = 1.37 $\mu F/cm^2$ as well
infinity and K = 8.8. The value of oxide thickness obtai
are given in Table 3.5. The effect of disregarding
interfacial capacitance amounts to over estimation of ox
thickness. Also, this method gives much higher values of

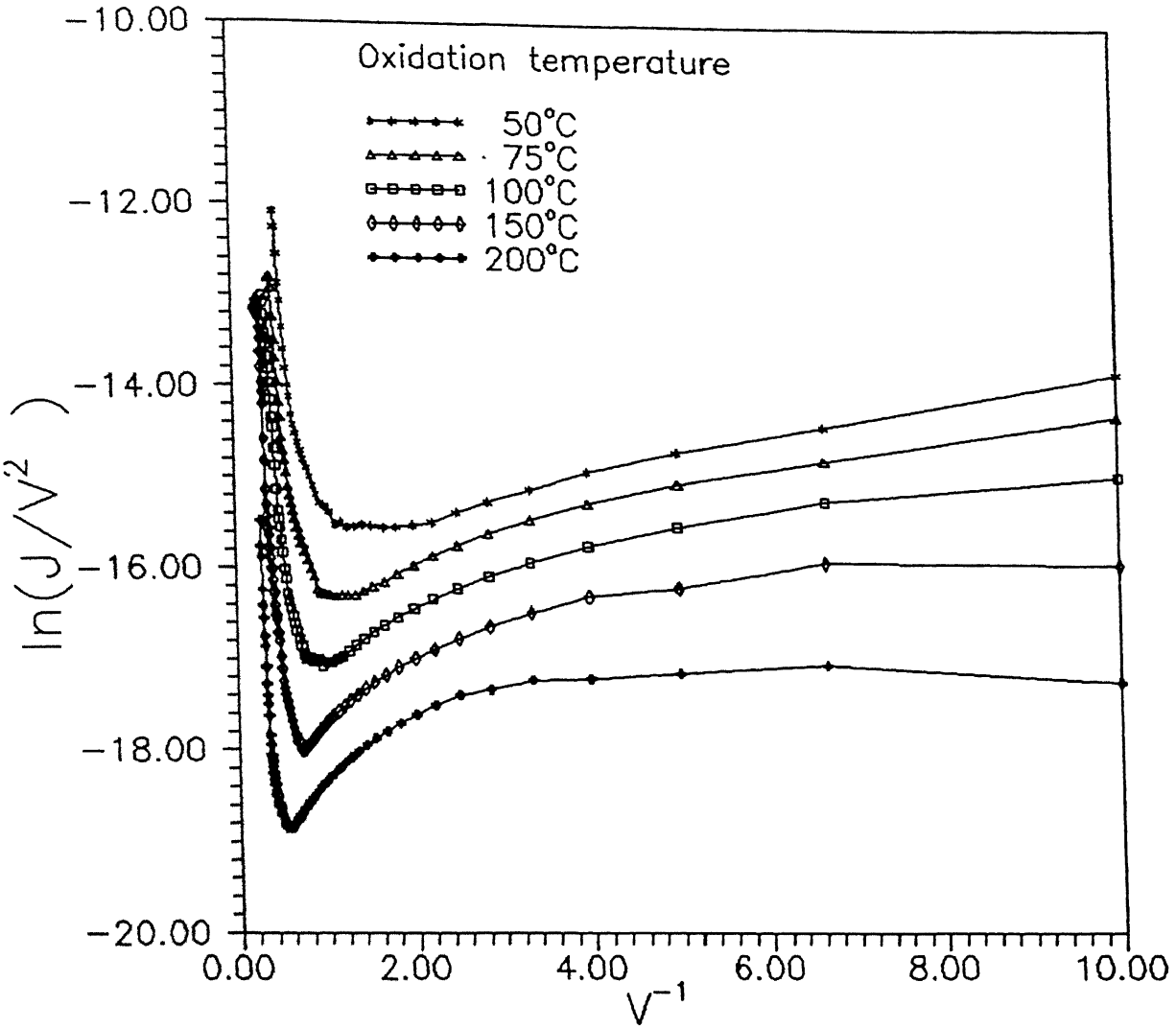

Fig. 3.6 Plot of $\ln(J/V^2)$ versus V^{-1} for Al-Al_2O_3-Al structures using data of Fig.3.2.

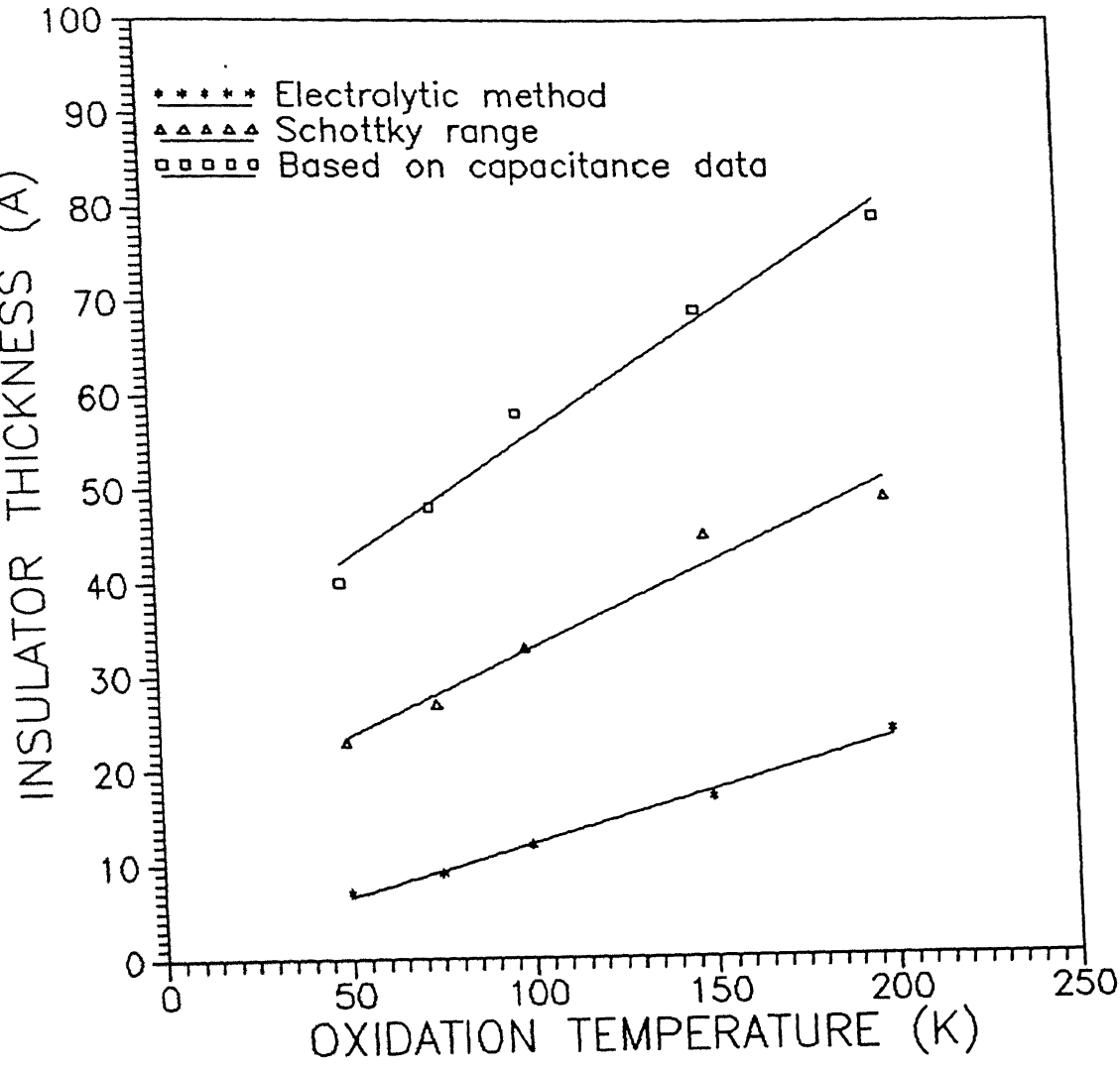

Fig. 3.7 Plots showing insulator thickness versus oxid temperature.

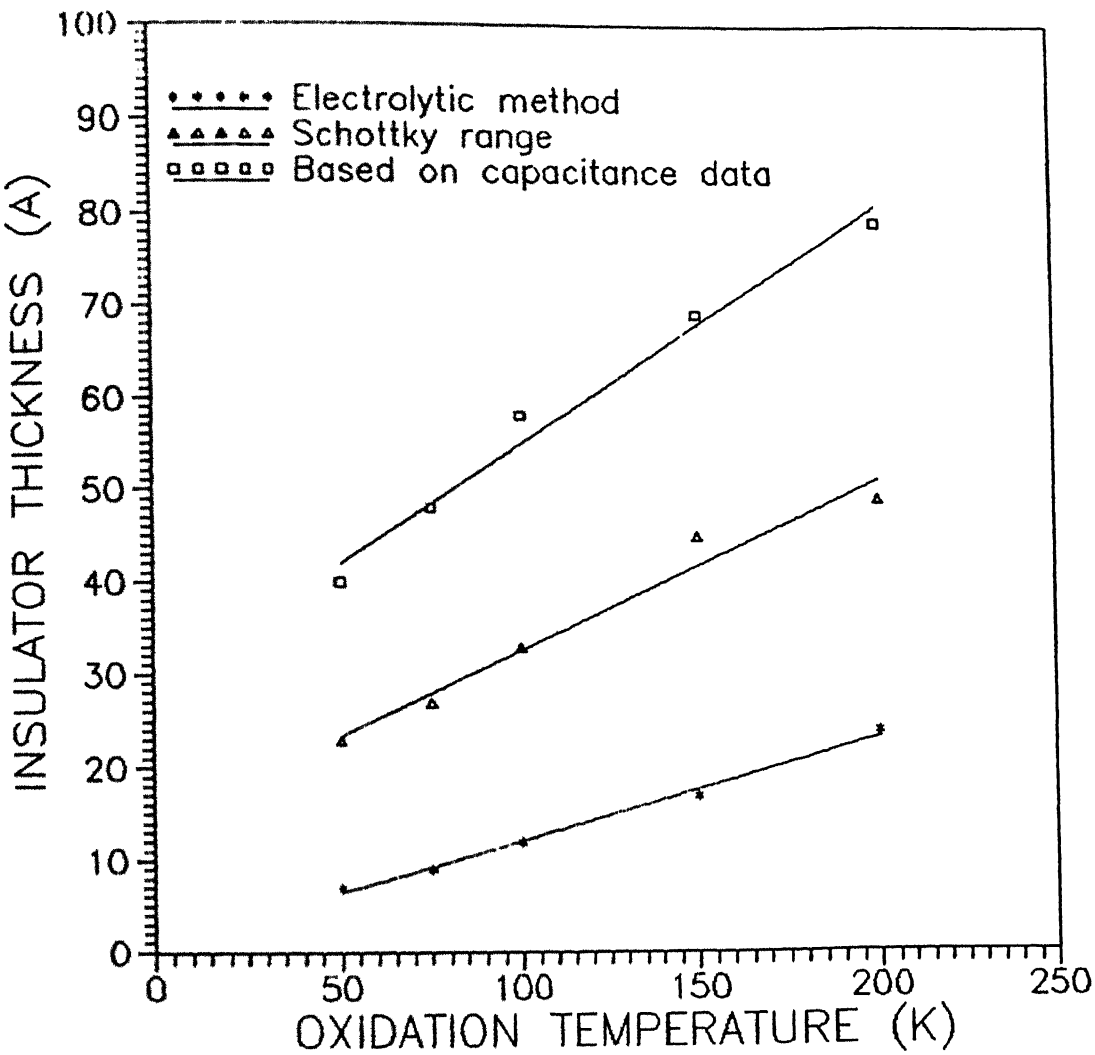

Fig. 3.7 Plots showing insulator thickness versus oxidation temperature.

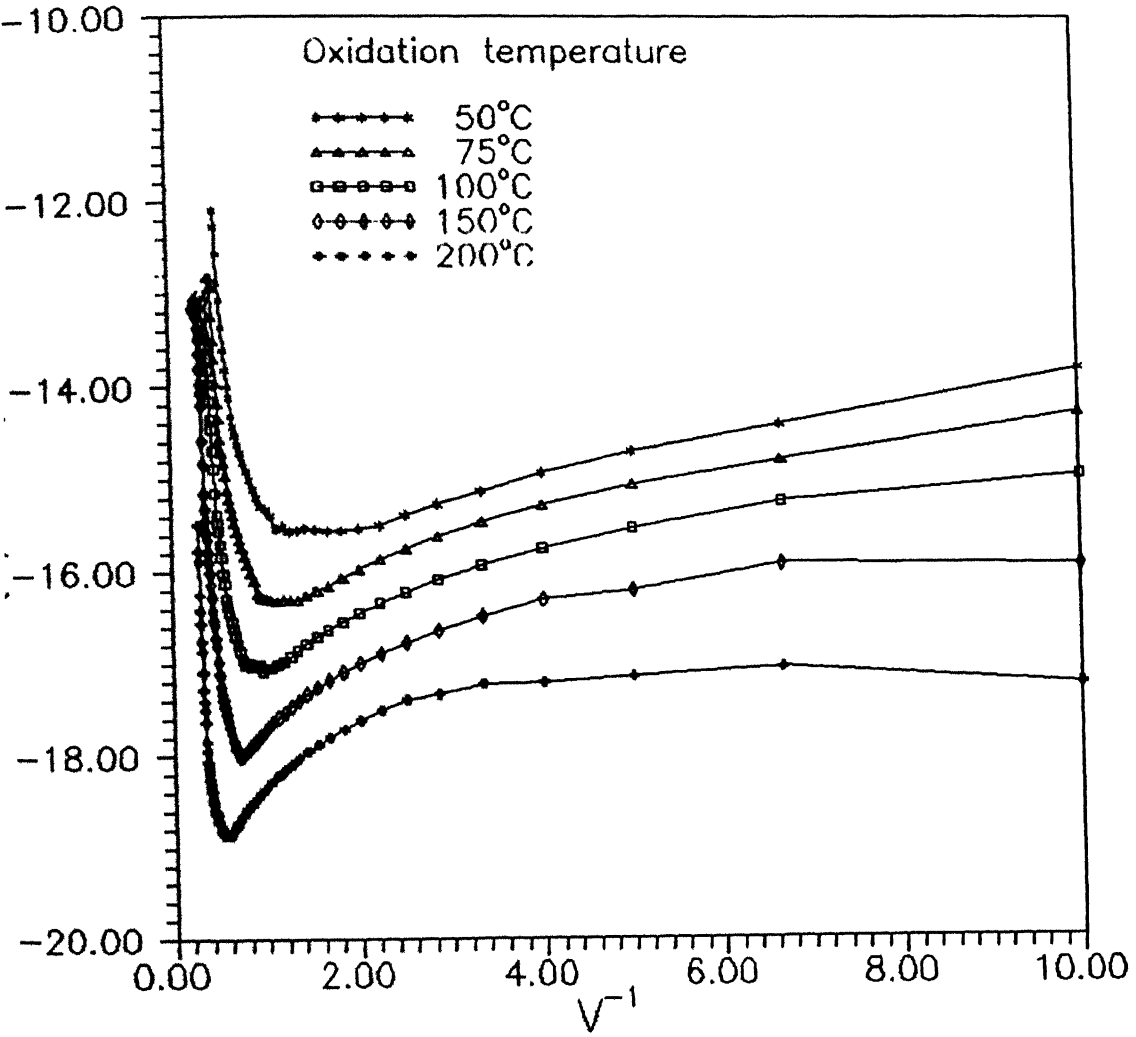

Fig. 3.6 Plot of $\ln(J/V^2)$ versus V^{-1} for Al-Al_2O_3-Al structures using data of Fig.3.2.

oxide thickness even with C_i/A= 1.37 $\mu F/cm^2$ when compared with data of Tables 3.3 & 3.4. This means that to have consistency in results the value of the interfacial capacitance should be much smaller, i.e., Ø.74 $\mu F/cm^2$.

The oxide thickness determined by electrolytic method described in Section 2.4 are given in Table 3.5. The values are significantly different than those found by capacitance measurements. It seems that the method is capable of detecting a particular portion of oxide only. This finding appears to be in line with that of Hunter and Fowle[23,24], who suggested two types of layers in thermally formed oxide : (a) compact layer near metal-oxide interface and (b) permeable layer at the oxygen-oxide interface. The thickness of the former is controlled by temperature alone, while that of later is a function of time and the destructive effects of the environment. The outer portion is formed by reaction of the compact oxide with the components of the environment, principally moisture. It is different from the compact oxide in the sense that it allows current to pass freely in either direction. May be we are just measuring the thickness of the compact layer itself. Or else, the method is not at all useful. This issue can not be resolved by the present data.

3.5 *Calculation of the effective mass of the electron*

We now calculate the effective mass[27] ($m^*=m/m_o$) of electron in thin Al_2O_3 films using current data of regions belonging to field assisted tunneling and Schottky emission. Let the slope

of the linear portion of ln J vs $V^{1/2}$ plot identified as Schottky emission region be $(slope)_{SE}$. Similarly, negative slope of straight line in $ln(J/V^2)$ vs V^{-1} plot corresponds to field assisted tunneling is $(slope)_{FT}$. The slope of the Schottky characteristics in ln $(J)-(V^{1/2})$ plots provide the product

$$\epsilon_s s_s = \frac{e^3}{4\pi(kT)^2(slope)_{SE}^2} \qquad .....3.3$$

and the slope of tunnel characteristics in $ln(J/V^2)-V^{-1}$ plots gives the thickness(s_T) as

$$s_T = \frac{3h}{8\pi(2m_o^* m)^{1/2}\,(slope)_{FT}\,\phi^{3/2}} \qquad .....3.4$$

where ϵ_s is the permitivity of the insulator. Substituting s_T from eq. (3.4) into eq. (3.3), for s_s, the value of m^* can be calculated. The values of $m^*(=m/m_o)$found this way have been listed in Table 3.6.

Table 5.2 Estimated values of ratio m/m_o

Annealing Temp.	$(slope)_{SE}$ (slope Shotttky region)	$(slope)_{FT}$ (slope tunnel region)	$m/m_o = m^*$
50	7.87	-23.22	0.59
75	7.66	-20.70	0.39
100	7.31	-18.34	0.23
150	6.89	-16.83	0.14
200	6.68	-12.83	0.06

CHAPTER 4

CONCLUSIONS

1. The oxide layer can be grown succesfully by thermal oxidation of the top portion of the aluminium films in the temperature range 50-200°C in air for making Al-Al_2O_3-Al trilayer structures.

2. The J-V characteristics of Al-Al_2O_3-Al structures are complex in nature and have three distinct regions. An Ohmic region involving marginal increase in current with voltage, a non-linear region with moderate and steep rise in current and an anomalous region of very high current with or without exhibiting negative resistence and fluctuations in the current at high voltages. Beyond Ohmic region, Schottky emission occurs and causes non-linearity in the I-V characteristics. Eventually, the above current transport results due to field assisted tunneling above 10^6 V/cm.

3. The oxide thickness values estimated from the J-V data in the Schottky emission and field assisted tunneling regions are quite consistent, lie in the range 20-50Å and increases linearly withthe oxidation temperature (50-200°C). The capacitance measurements of Al-Al_2O_3-Al suggest the presence of the interfacial capacitance $\sim$ 0.74 $\mu F/cm^2$. The electrolyte method fails to determine the total oxide thickness and is perhaps

sensitive to a very specific region as the resulting thickness values are invariably found to be very small.

4. The effective barrier heights correspond to 0.82-0.87eV and 1.73-1.85eV for the Schottky emission and tunneling process, respectively. Both set of values increase with the oxide thickness.

5. The effective mass of the electron decreases with increase in the oxide thickness.

REFERENCES

1. T.E. Hartman,J.C. Blair, and C.A. Mead, *Thin Solid Films*, 2:79(1968).
2. P. L. Young, *J. Appl. Phys.*, 46:2794(1975).
3. J. Maserjian, and C. A. Mead, *J. Phys. Chem. Solids*, 28:1971(1967).
4. F. M. Nazar, *Thin Solid Films*, 51:L41(1978).
5. C. A. Mead, *J. Appl. Phys.*, 32:646(1961).
6. T.E. Hartman, and J.S. Chivian, *Phys.Rev.*, 134:A1094(1964).
7. E. Murphy and R.H. Good, *Phys. Rev.*, 102:1464(1956).
8. R.Holm, *J. Appl. Phys.*, 22:569(1951).
9. R.Stratton, *J. Appl. Phys. and Chem. of Solids*, 23:1177(1962).
10. S.R. Pollack and C.R. Morris, *J. Appl. Phys.*, 35:1503(1964).
11. J.G. Simmons, *J. Appl. Phys.*, 34:2581(1953).
12. C.M. Vodanicharov and S.G. Christov, *Solid State Electronics*, 15:933(1972).
13. D.V. Geppert, *J. Appl. Phys.*, 34:646(1963).
14. E.I. Maissel and H. Glang (eds.), *Handbook of Thin F Technology*, Mc Graw Hill, New York, 1970.
15. T.E. Hartman, *J. Appl. Phys.*,35:3283(1964).
16. S. R. Pollack, *J. Appl. Phys.*, 34:877(1963).
17. J.G. Simmons, *J. Appl. Phys.*,35:2472(1964).
18. H.Birey, *J. Appl. Phys*, 48:5209(1977).
19. D. Meyerhoffer and S.A. Ochs, *J. Appl. Phys.*, 34:2535(1963).
20. T. W. Hickmott, *J. Appl. Phys.*, 35:2679(1964)
21. J.G.Simmons , *J. Appl. Phys.*, 34:1793(1963).
22. D.R. Lamb, *Electrical Conduction Mechanisms in Thin Films* Hirst Research centre, Wembley, 1967.
23. M.S. Hunter, and P.Fowle, *J.Electrochemical Soc.*, 104:514(1954).
24. M.S. Hunter, and P.Fowle, *J.Electrochemical Soc.*, 104:481(1954).
25. K.R.Lawless, *Rep. Prog. Phys.*, 37:231(1974).
26. Anand Madhukar, *Current-voltage characteristics of Al-Al_2O_3 structures*, M.Tech. thesis, Indian Institute of Technology, Kanpur (1996).
27. J. Antula, *Phys. Stat. Sol.*, 24:89(1967).

28. G. Dearnley, A.H. Stoneham, and D.V. Morgan, *Rep. Prog. Phy.*, 33:1129(1970).

29. S.R. Polack and J.A. Seitchik, *Appl. Solid State Science*, Vol.-1, R. Wolfe and Kriessman (eds.) Academic Press, New York, 1969.

30. A.F. Hebard , S.A. Ajuria, R.H. Eick, *Appl. Phys. Lett.*, 51:1349(1987).